



CROSS-MODEL VERIFICATION OF WALL-BOUNDED FLOWS USING FINITE-JAX

Arturo Rodriguez^{1*}, Avinash Potluri¹, Aryan Singh², Vyom Kumar³, Kate Reza⁴, Francisco O. Aguirre Ortega¹, Vineeth Vijaya Kumar¹, Noah L. Estrada¹

¹Texas A&M University - Kingsville, Kingsville, TX 78363, USA

²Casady School, Oklahoma City, OK 73120, USA

³Moreau Catholic High School, Hayward, CA 94544, USA

⁴University of Texas at El Paso, El Paso, TX 79968, USA

ABSTRACT

Accurate prediction of wall-bounded flows remains central to advancing both theoretical understanding and computational methods in fluid mechanics. In this study, we perform a numerical simulation of channel flow using a complementary approach: a high-performance, differentiable finite-difference solver developed in JAX (Finite-JAX) and an analytical solution derived from the Navier-Stokes Equations, also referred to as the Hagen-Poiseuille equation. The solver is applied to the incompressible Navier-Stokes equations, along with appropriate boundary conditions, to capture canonical flow features such as velocity profiles and pressure gradients. Cross-model verification is conducted by systematically comparing numerical results between Finite-JAX and the analytical solution, with a focus on velocity distributions. In addition, numerical results are benchmarked against analytical solutions for laminar regimes, allowing for the direct quantification of verification accuracy errors. Our findings demonstrate that cross-model verification not only strengthens confidence in simulation fidelity but also provides a pathway for integrating differentiable solvers with established computational fluid dynamics platforms, paving the way for future fluid flow research.

KEY WORDS: JAX, Scientific Computing, High-Performance Computing, Finite Difference, Bounded Flows

NOMENCLATURE

Variables

\vec{u}	velocity vector	m/s
t	time	S
ρ	density	kg/m ³
p	pressure	Pa
ν	kinematic viscosity	m ² /s
F	forcing	
u	velocity in the x-direction	m/s
v	velocity in the y-direction	m/s
x	x-component of direction	m
y	y-component of direction	m
u	solution of the x-component	
μ	dynamic viscosity	Pa s
H	y-direction of the channel/pipe	M
L	loss	
CFL	courant number	

Subscripts and Superscripts

x	x-coordinate
y	y-coordinate
ana	analytical solution
2	l2 norm
i	x-index
j	y-index
n	time-index
max	max value

*Corresponding Author: arturo.rodriguez@tamuk.edu

v solution of the y -component

1. INTRODUCTION

The accuracy of continuous-wall flow modeling poses a challenge in fluid mechanics, with applications ranging from aerospace vehicle design and pipe flow transport to biomedical flows and energy systems. Despite the simplicity of canonical configurations, channel flow demonstrates the complexities of boundary layer physics, including the interplay between viscous and inertial forces, the emergence of velocity gradients, and the dependence of flow behaviour on the Reynolds number scale [1,2,3]. As such, it frequently serves as a validation case for numerical methods and the use of turbulence models [4].

In recent decades, advances in computational fluid dynamics (CFD) have significantly enhanced the accuracy of simulations of wall-bounded flows [5]. Commercial software, such as ANSYS Fluent, has been widely adopted in industry and academia due to its mature finite volume method, robust solvers, and the extension of turbulence models [6]. In parallel, advancements in programming have introduced a new class of solvers, facilitated by platforms such as JAX, TensorFlow, and PyTorch, which are designed for high-performance computing while also supporting machine learning workflows [7, 8]. These solvers are particularly attractive for modern applications involving uncertainty quantification, data assimilation, and physics-informed neural networks (PINNs) [9, 10, 11, 12].

The emergence of numerical solvers, such as Finite-JAX—a high-performance, finite-difference CFD code developed in JAX—offers a way to integrate traditional numerical methods with differentiable programming capabilities [13, 14, 15, 16, 17, 18]. However, the reliability of these frameworks first requires systematic verification and validation against established commercial solvers and analytical solutions. Model-to-model verification provides a structured approach to evaluating new high-fidelity tools, ensuring that predictions are consistent with those of validated CFD software across scenarios from a range of canonical flows.

In this work, we conduct a comprehensive study of channel flows, verifying the results using Finite-JAX and the analytical solution. The solvers are applied to the incompressible Navier-Stokes equations with surface conditions that capture flow characteristics, including velocity distributions and pressure gradients. Results are compared against analytical solutions in the laminar regime. Through this procedure, we can quantify the verification accuracy, establish confidence in the Finite-JAX differentiable CFD solver, and highlight the complementary roles of traditional and differentiable solvers in advancing the study of wall-bounded flows.

2. METHODS & EQUATIONS

We solve the incompressible Navier-Stokes equations in 2-D (channel flow with periodicity in the stream direction, no-slip walls above and below), with the streamwise constant a body force F (equivalent to a uniform pressure gradient):

$$\frac{\partial \vec{u}}{\partial t} + (\vec{u} \cdot \nabla) \vec{u} = -\frac{1}{\rho} \nabla p + \nu \nabla^2 \vec{u} + F \hat{e}_x \quad (1)$$

$$\nabla \cdot \vec{u} = 0 \quad (2)$$

Where $\vec{u} = (u, v)$, density ρ , kinematic viscosity ν , and F is a constant acceleration in the x -direction. In a fully developed laminar channel driven by a constant $-\partial p / \partial x$, the code sets $\partial p / \partial x = -\rho F$ so that the forcing term $F \hat{e}_x$ represents the pressure gradient.

2.1 Chorin Projection Operator Splitting Method

To enforce incompressibility at each step, the code uses a projection-splitting method introduced by Chorin, which uses the Poisson equation, which discretizes the source term b and assembles it with the following discretization:

$$\nabla^2 p = \rho \left[\frac{1}{\Delta t} \nabla \cdot \vec{u} - (\partial_x u)^2 - 2(\partial_y u)(\partial_x v) - (\partial_y v)^2 \right] \quad (3)$$

On the grid (interior),

$$b_{j,i} = \rho \left[\frac{1}{\Delta t} \left(\frac{u_{j,i+1} - u_{j,i-1}}{2\Delta x} + \frac{v_{j+1,i} - v_{j-1,i}}{2\Delta y} \right) - \left(\frac{u_{j,i+1} - u_{j,i-1}}{2\Delta x} \right)^2 - 2 \left(\frac{u_{j,i+1} - u_{j,i-1}}{2\Delta x} \right) \left(\frac{v_{j+1,i} - v_{j-1,i}}{2\Delta y} \right) - \left(\frac{v_{j+1,i} - v_{j-1,i}}{2\Delta y} \right)^2 \right] \quad (4)$$

With this b , the pressure Poisson equation is discretised (five-point stencil) as:

$$\frac{p_{j,i+1} - 2p_{j,i} + p_{j,i-1}}{\Delta x^2} + \frac{p_{j+1,i} - 2p_{j,i} + p_{j-1,i}}{\Delta y^2} = b_{j,i} \quad (5)$$

Rearranged for Jacobi/Gauss-Seidel iteration:

$$p_{j,i} \leftarrow \frac{(p_{j,i+1} + p_{j,i-1})\Delta y^2 + (p_{j+1,i} + p_{j-1,i})\Delta x^2 - b_{j,i}\Delta x^2\Delta y^2}{2(\Delta x^2 + \Delta y^2)} \quad (6)$$

Boundary conditions for p :

- Periodic in x : values at $i = -1$ and $i = 0$ wrap to $i = n_x - 2$ and $i = n_x - 1$ (implemented explicitly for the first/last columns).
- Neumann at walls $y = 0, H$: $\partial p / \partial y = 0 \rightarrow p_{0,i} = p_{1,i}, p_{n_y-1,i} = p_{n_y-2,i}$.

2.2 Velocity – Momentum Step

After solving pressure, we proceed to calculate velocities explicitly using Euler's method, employing central differences for convection, the pressure gradient, and diffusion. For interior nodes:

$$u_{j,i}^{n+1} = u_{j,i}^n - u_{j,i}^n \frac{\Delta t}{\Delta x} (u_{j,i}^n - u_{j,i-1}^n) - v_{j,i}^n \frac{\Delta t}{\Delta y} (u_{j,i}^n - u_{j-1,i}^n) - \frac{\Delta t}{2\rho\Delta x} (p_{j,i+1} - p_{j,i-1}) + v\Delta t \left[\frac{u_{j,i+1}^n - 2u_{j,i}^n + u_{j,i-1}^n}{\Delta x^2} + \frac{u_{j+1,i}^n - 2u_{j,i}^n + u_{j-1,i}^n}{\Delta y^2} \right] + F\Delta t \quad (7)$$

$$v_{j,i}^{n+1} = v_{j,i}^n - u_{j,i}^n \frac{\Delta t}{\Delta x} (v_{j,i}^n - v_{j,i-1}^n) - v_{j,i}^n \frac{\Delta t}{\Delta y} (v_{j,i}^n - v_{j-1,i}^n) - \frac{\Delta t}{2\rho\Delta x} (p_{j,i+1} - p_{j,i-1}) \quad (8)$$

$$+ v\Delta t \left[\frac{v_{j,i+1}^n - 2v_{j,i}^n + v_{j,i-1}^n}{\Delta x^2} + \frac{v_{j+1,i}^n - 2v_{j,i}^n + v_{j-1,i}^n}{\Delta y^2} \right]$$

Boundary conditions for u:

- No-slip walls $y = 0, H$: $u = 0, v = 0$ at $j = 0$ and $j = n_y - 1$.
- Periodic in x: values at $i = 0$ and $i = n_x - 1$ are updated using wrapped neighbors.

2.3 Stopping Criterion

$$udiff = \frac{\sum u^n - \sum u^{n-1}}{\sum u^n} < 10^{-6} \quad (9)$$

2.4 Analytical Benchmark | Plane Poiseuille Profile

With constant $-\partial p/\partial x = \rho F$ and no-slip at $y = 0, H$, the steady laminar solution is:

$$u_{ana}(y) = -\frac{1}{2\mu} \frac{\partial p}{\partial x} y(y-H) = -\frac{\rho F}{2\mu} y(y-H) \quad (10)$$

$$v_{ana} = 0 \quad (11)$$

The code compares the numerical solution $u(y)$ at a mid-plane $x = const$ to $u_{ana}(y)$, and reports the error:

$$L_2(u) = \left(\frac{1}{N} \sum_k [u_k - u_{ana}(y_k)]^2 \right)^{1/2} \quad (12)$$

$$\max |u - u_{ana}| \quad (13)$$

$$\min |u - u_{ana}| \quad (14)$$

2.5 Stability

- Spatial operators are second-order accurate (central differences); time integration is first-order.
- Stability requires a suitable step obeying a CFL-like restriction combining convection and diffusion:

$$\Delta t \leq \min \left(\frac{CFL\Delta x}{|u|_{max}}, \frac{CFL\Delta y}{|v|_{max}}, \frac{CFL_v}{v}, \frac{\Delta x^2 \Delta y^2}{\Delta x^2 + \Delta y^2} \right) \quad (15)$$

With typical choices, CFL, $CFL_v \leq 0.5$ for robustness.

3. RESULTS AND DISCUSSION

This contour plot presents the numerical solution of the stream flow velocity component, $u(x, y)$, in the canonical two-dimensional channel flow. The color map displays the velocity magnitude, with the darkest color indicating low velocity near the wall, where the velocity is zero, and the lightest color representing the stream flow velocity. The distribution reveals a parabolic velocity profile, consistent with the classical pressure-driven Poiseuille flow solution. The velocity decreases near the walls due to the no-slip condition, increases monotonically through the shearing layers, and reaches a maximum velocity at the channel center.

What is particularly interesting in this figure is the invariance of the velocity contours along the flow direction. They are spatially uniform and reflect the state of fully developed flow, where streamwise gradients vanish and the dynamics reduce to a balance between pressure forcing and viscous dissipation. The color bar quantifies the velocity magnitude, ranging from zero at the wall to the free stream at the center, which agrees with the theoretically derived analytical solution and the expectations of the forcing.

This result highlights the solver's ability to recover the fundamental benchmark of incompressible fluid mechanics. The parabolic structure here evidently serves not only as a verification of the numerical discretization and boundary conditions, but also as a demonstration that simple geometries capture the essence of viscous transport phenomena. Broadly speaking, this simulation serves as a step toward more complex scenarios—such as unsteady, turbulent, or non-Newtonian—where deviations from parabolic patterns enrich the Multiphysics scale of flows between walls.

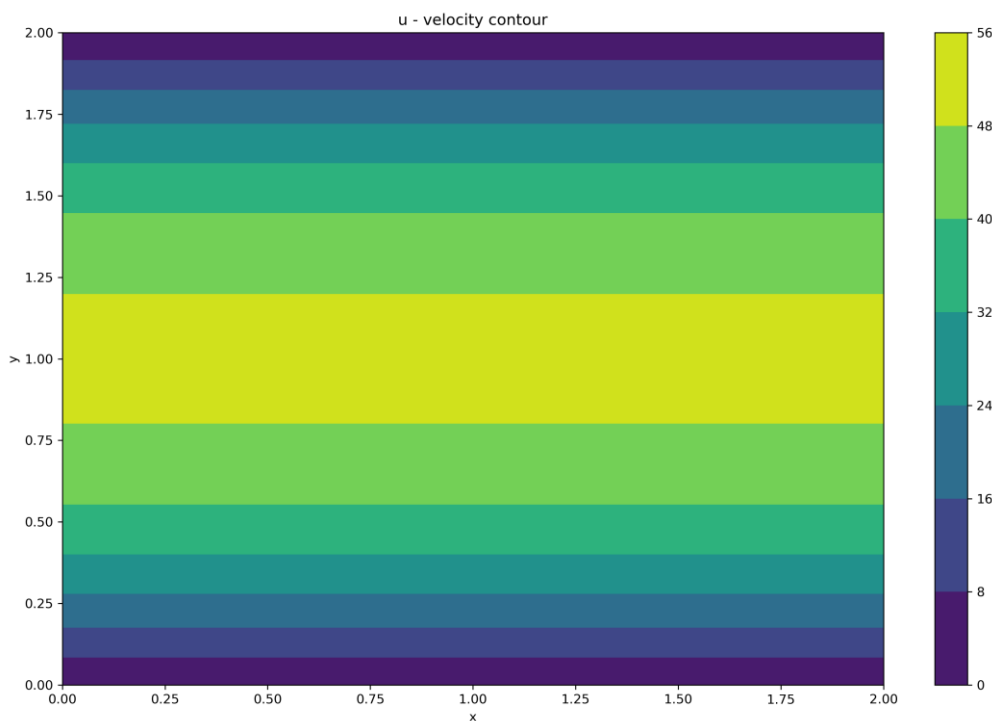


Fig. 1. Channel Flow Contour

Table 1. Error Norms

L2 Norm	Max Norm	Min Norm
1.4765e-02	2.1140e-02	0.0000e+00

Figure 2 illustrates a direct comparison between the analytical solution of a developed Poiseuille flow and the numerical solution obtained by a JAX-based CFD solver. The horizontal axis represents the velocity component u , and the vertical axis represents the wall normal at the y -coordinate, extending from $y = 0$ to $y = 2$, which corresponds to the channel height. The analytical profile shows discrete points, and the numerical solution represents a continuous curve.

The parabolic shape of the velocity distribution is immediately apparent. The velocity vanishes at the surfaces, reflecting the no-slip condition at the surface, which increases to a maximum velocity at the channel centre. This demonstrates pressure-driven laminar channel flow, where the balance between viscous diffusion and the imposition of the pressure gradient is evident, exhibiting a quadratic dependence on the y -axis. What is notable is the agreement between the two curves: the numerical solution obtained by coupling pressure and velocity reproduces the analytical results almost exactly, with a deviation that is imperceptible to the eye.

The agreement not only validates the correctness of the discretization and surface conditions but also the implementation in the JAX solver, which faithfully captures the precision of the Poisson scheme, thereby preserving the incompressibility of fluid dynamics. This figure provides a strong benchmark; if the solver can replicate the canonical profile with high accuracy, one gains confidence in its application in more complex settings where analytical solutions do not exist. In the context of computational fluid dynamics, verification of fundamental solutions is essential before extending numerical methods to transition and turbulent regimes.

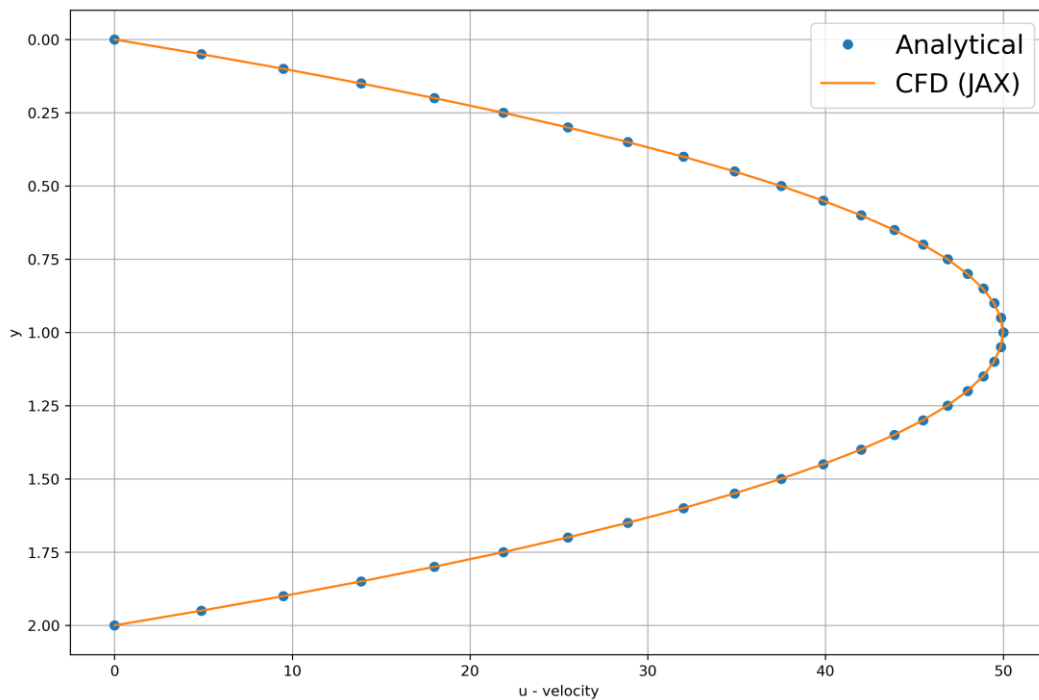


Fig. 2. Channel Flow Numerical vs. Analytical Solutions

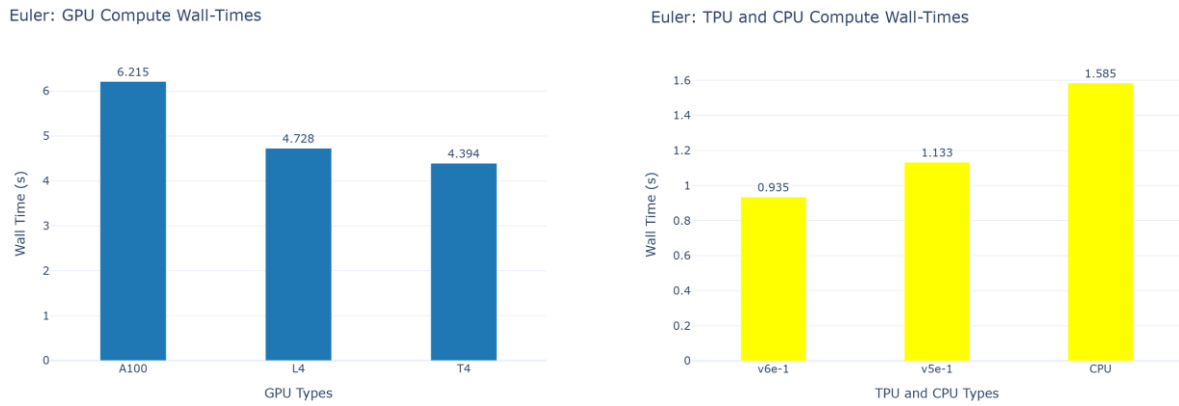


Fig. 3 and 4. Euler: GPU, TPU, and CPU Compute Wall-Times

These two figures present a quantitative comparison of the wall times for computing the Euler discretization on different hardware accelerators. The left figure reports GPU-based performance, while the right figure corresponds to TPU and CPU execution times. The vertical axis shows the wall time in seconds, serving as a measure of computational efficiency, and the horizontal axis identifies the hardware platform on which the code runs.

In the computing benchmarks, three architectures are examined: the A100, L4, and T4 GPUs. Somewhat counterintuitively, the A100, being the flagship of GPU performance, takes the longest computation time, approximately 6.2 seconds, although the smaller T4 card yields faster results at approximately 4.4 seconds. The L4 takes approximately 4.7 seconds, which is in the middle of the two. The inversion of expectations demonstrates the interplay between algorithm structure, memory access patterns, and GPU architecture. This reflects the fact that capability does not translate proportionally to speedups, particularly for the structure of discrete Euler PDE solvers.

The TPU and CPU benchmarks reveal a complementary comparison. The v6e-1 TPU achieves the shortest computational time, approximately 0.935 seconds, which is less than the v5e-1 TPU (1.133 seconds) and the CPU (1.585 seconds). Here, hierarchical preemption is preserved: tensor processing is faster than general-purpose CPUs. The difference between v6e-1 and v5e-1 illustrates the gains in the hierarchy of successive generations of TPUs, offering reduced computation time for PDEs.

Together with the figures, this lesson is essential for scientific computing: performance is not only dictated by peak FLOP counts, but also by the emergence of hardware design, memory hierarchy, and algorithm structure. For PDE solvers, these results demonstrate the need for portable algorithms that efficiently adapt to heterogeneous architectures, thereby enhancing the fidelity and speed of simulations of flows and other applications.

4. CONCLUSION

A two-dimensional incompressible Navier–Stokes solver based on the Chorin projection method was developed and validated for wall-bounded flows. The numerical formulation successfully captured velocity gradients in the boundary layer, with plane Poiseuille flow serving as a verification case. The stability limits imposed by the CFL condition were confirmed, and the efficiency of Jacobi and Gauss–Seidel iterations in solving the pressure Poisson equation was demonstrated.

Beyond classical CFD methods, this work highlights the advantages of integrating modern computational frameworks, such as JAX, into traditional solvers. These platforms enable scalable, differentiable simulations and provide a pathway toward machine learning-accelerated CFD. Future studies will extend the solver to three-dimensional turbulence, incorporate GPU-based acceleration, and develop hybrid ML–CFD strategies for large-scale wall-bounded flow applications.

ACKNOWLEDGMENT

This project utilized Prof. Arturo Rodriguez's Startup funds, which Texas A&M University-Kingsville, the Department of Mechanical and Industrial Engineering, and the College of Engineering granted.

REFERENCES

- [1] Moser, R. D., Kim, J., & Mansour, N. N. (1999). Direct numerical simulation of turbulent channel flow up to $Re=590$. *Phys. fluids*, 11(4), 943-945.
- [2] Kim, J., Moin, P., & Moser, R. (1987). Turbulence statistics in fully developed channel flow at low Reynolds number. *Journal of fluid mechanics*, 177, 133-166.
- [3] Tatsumi, T., & Yoshimura, T. (1990). Stability of the laminar flow in a rectangular duct. *Journal of Fluid Mechanics*, 212, 437-449.
- [4] Tsukahara, T., & Kawamura, H. (2014). Turbulent heat transfer in a channel flow at transitional Reynolds numbers. *arXiv preprint arXiv:1406.0959*.
- [5] Bose, S. T., & Park, G. I. (2018). Wall-modeled large-eddy simulation for complex turbulent flows. *Annual review of fluid mechanics*, 50, 535-561.
- [6] Jia, R., Kamel, M. S., Wu, C., & Agrawal, B. (2025). Ansys Fluent HPC for Large-Scale CFD Simulations. In *AIAA SCITECH 2025 Forum* (p. 1950).
- [7] Brunton, S. L., Noack, B. R., & Koumoutsakos, P. (2020). Machine learning for fluid mechanics. *Annual review of fluid mechanics*, 52(1), 477-508.
- [8] Rodriguez, A., Chattopadhyay, A., Kumar, P., Rodriguez, L. F., & Kumar, V. (2024). Partition of Unity Physics-Informed Neural Networks (POU-PINNs): An Unsupervised Framework for Physics-Informed Domain Decomposition and Mixtures of Experts. *arXiv preprint arXiv:2412.06842*.
- [9] Eivazi, H., Tahani, M., Schlatter, P., & Vinuesa, R. (2022). Physics-informed neural networks for solving Reynolds-averaged Navier–Stokes equations. *Physics of Fluids*, 34(7).
- [10] Wu, J. L., Xiao, H., & Paterson, E. (2018). Physics-informed machine learning approach for augmenting turbulence models: A comprehensive framework. *Physical Review Fluids*, 3(7), 074602.
- [11] Yang, X. I. A., Zafar, S., Wang, J. X., & Xiao, H. (2019). Predictive large-eddy-simulation wall modeling via physics-informed neural networks. *Physical Review Fluids*, 4(3), 034602.
- [12] Raissi, M., Perdikaris, P., & Karniadakis, G. E. (2019). Physics-informed neural networks: A deep learning framework for solving forward and inverse problems involving nonlinear partial differential equations. *Journal of Computational physics*, 378, 686-707.
- [13] Bradbury, J., Frostig, R., Hawkins, P., Johnson, M. J., Leary, C., Maclaurin, D., ... & Zhang, Q. (2018). JAX: composable transformations of Python+ NumPy programs.
- [14] Shang, W., Zhou, J., Panda, J. P., Xu, Z., Liu, Y., Du, P., ... & Luo, T. (2025). JAX-BTE: a GPU-accelerated differentiable solver for phonon Boltzmann transport equations. *npj Computational Materials*, 11(1), 129.
- [15] Bezgin, D. A., Buhendwa, A. B., & Adams, N. A. (2023). JAX-Fluids: A fully-differentiable high-order computational fluid dynamics solver for compressible two-phase flows. *Computer Physics Communications*, 282, 108527.
- [16] Bezgin, D. A., Buhendwa, A. B., & Adams, N. A. (2025). JAX-Fluids 2.0: towards HPC for differentiable CFD of compressible two-phase flows. *Computer Physics Communications*, 308, 109433.
- [17] Xue, T., Liao, S., Gan, Z., Park, C., Xie, X., Liu, W. K., & Cao, J. (2023). JAX-FEM: A differentiable GPU-accelerated 3D finite element solver for automatic inverse design and mechanistic data science. *Computer Physics Communications*, 291, 108802.
- [18] Wang, W., Zhang, X., Bezgin, D., Buhendwa, A., Chu, X., & Weigand, B. (2024). JAX-based differentiable fluid dynamics on GPU and end-to-end optimization. *arXiv preprint arXiv:2406.19494*.

APPENDIX

<i>Name</i>	<i>Symbol</i>	<i>Value</i>	<i>Units</i>	<i>Notes</i>
Grid points in x	nx	41	-	Number of nodes along x
Grid points in y	ny	41	-	Number of nodes along y
Pressure Poisson Iterations	nit	80	-	Jacobi-like iterations per pressure solve
Domain Height	H	2.0	m	Domain spans
Grid spacing in x	dx	0.05	length	Uniform spacing
Grid spacing in y	dy	0.05	length	Uniform spacing
Density	rho	2.0	kg/m ³	Fluid density
Kinematic viscosity	nu	0.01	m ² /s	Viscosity is used in momentum diffusion
Dynamic viscosity	mu	0.02	Pa-s	Appears in analytical solution
Body-force acceleration	F	1.0	m/s ²	Constant x-direction forcing

Pressure gradient	dpx	2.0	Pa/m	Equivalent constant dpx driving the flow
Time step	dt	0.1	s	Explicit update step for u,v
Initial u field	u0	zeros((ny,nx))	-	Starts at rest
Initial v field	v0	zeros((ny,nx))	-	Starts at rest
Initial pressure	p0	ones((ny,nx))	-	Uniform initial guess
Convergence tolerance	tol	1e-6	-	Relative change threshold on sum(u)
Max iteration steps	max_steps	100000	-	Safety cap for while-loop convergence
JAX precision	jax_enable_x64	True	-	Use float64 for better stability
JAX platform	jax_platform_name	cpu	-	Can be changed to "gpu" if available